PORT SAID ENGINEERING RESEARCH JOURNAL
Faculty of Engineering - Port Said University
Volume 29 No. 3 pp: 38:51

Seismic Response of Tunnels in Soft Soil under Various Earthquakes

Ahmed Sayed Hegazey [1,], Kamal Mohamed Hafez [2], Walid Hamdy El Kamash [3], Azza Hassan Moubarak [4].*

[1*] MCs candidate Civil Engineering Department, Suez Canal University, Ismailia, Egypt, email: ahmed.sayed@eng.suez.edu.eg
[2] Professor, Geotechnical, Foundation Engineering Department, Faculty of Engineering, Suez Canal University, Ismailia, Egypt, email: Kamal.hafez@eng.suez.edu.eg,
[3] Professor, Geotechnical, Foundation Engineering Department, Faculty of Engineering, Suez Canal University, Ismailia, Egypt, email: waleedelkamash@eng.suez.edu.eg,
[4] Associate Professor, Civil Department, Faculty of Engineering, Suez Canal University, Ismailia, Egypt, email: Azza_moubarak@eng.suez.edu.eg .
*Corresponding author, DOI: 10.21608/pserj.2025.368225.1399

Received 16-3-2025,
Revised 23-4-2025,
Accepted 12-5-2025

ABSTRACT

Earthquakes can cause significant damage to infrastructure or buildings. This study investigates the seismic response of segmented tunnels through numerical analysis under various earthquake conditions. The research examines ring and longitudinal behavior at 10m depth using four distinct loading scenarios: static lining phase and three earthquake events (Petrolia, Elcentro, and Geysers). The behavior of a shallow tunnel in soft soil is simulated using PLAXIS 3D. The tunneling study employs a constitutive model based on typical implementations of the hardening soil model (HSM). The settlement effects are as follows: the settlement was more significant for the Petrolia earthquake than the El Centro earthquake. Vertical displacement analysis shows a maximum displacement of 299mm due to the Petrolia earthquake loading. The longitudinal analysis demonstrates complex wave propagation effects, with maximum moments occurring at approximately 12m length and significant variations between 20 and 40m. The results show that high-frequency earthquakes, such as the Petrolia earthquakes, induce considerable alterations of pore water pressure and cause significant settlement of soft soils. In addition, it is determined in the study that, given the same driving force, an earthquake of different magnitudes has different characteristics to initiate the deformation of the tunnel lining, and the deformation of the tunnel's crown is the largest. The results highlight the critical importance of seismic loading characteristics in tunnel design, particularly in soft soil conditions.

Keywords: Shield tunnel, Seismic response, Soft soils, PLAXIS 3D numerical simulation, Hardening soil model.

1.INTRODUCTION

Most shield-driven tunnels are supported by segmental linings, which provide the structural capacity to resist ground and water pressures and the necessary framework to advance the shield machine. Longitudinal joints connect a certain number of segments to form a ring, and then several rings are connected by circumferential joints to complete the lining (see Figure 1) [1]. The dynamic characteristics of the soil layer response to seismic activity and the soil stiffness are critical in determining whether the seismic loading is of concern. Underground transportation infrastructure, particularly shield-driven tunnels, has become increasingly vital in urban development. The seismic performance of these structures, especially in soft soil conditions, presents complex engineering challenges that require sophisticated three-dimensional numerical analysis. While underground structures generally experience less seismic damage than surface structures, the intricate interaction between segmented tunnel linings and surrounding soil during earthquakes demands advanced

computational modeling approaches. This paper presents a systematic investigation combining theoretical analysis with advanced numerical modeling using PLAXIS 3D to provide deeper insights into seismic effects on segmented tunnels in soft soils, mainly focusing on the three-dimensional aspects of tunnel response that conventional two-dimensional analyses cannot capture [2]. Earthquakes tend to inflict less magnitude of damage on subsurface structures and more on surface structures [3]. Some scholars are researching using the finite element method to understand the multidirectional seismic loading effects on the shield tunnel segment opening [4]. They identified the boundaries for the maximum segment opening at various depths for seismic loading and anticipated the maximum segment opening at multiple depths for seismic loading. *Gharehdash et al.* focused on the impact of dynamic responses of shield tunnels buried in soft soil under vibrating loads, which induce significant dynamic reactions in the tunnel lining structure and its soft foundation [5]. *Zheng et al.* explored the nonlinear dynamic responses of tunnels under longitudinal seismic action. They studied the influences of P-wave velocity in soil and the tunnel segment bolting stiffness parameter on internal force and deformation under nonlinear soil-structure interaction [6]. Their findings conclude that this will increase relative displacement between the tunnel structure and the soil, leading to nonlinear stress regime systems, which cause greater stress concentration in the structures. The tunnel linings earthquakes study was devoted to the static load and dynamic load impact on them, the wide range of tunnel diameters, and the elasticity response conditions [7]. Although dynamic stress was less hazardous than other factors, it is not negligible for underground structures. Also, *Chen et al.* utilized longitudinal seismic response analysis and vertical seismic motions to simulate submarine tunnels in soft marine environments for future subsea tunnel construction [8]. *Cabangon et al.* used 2D and 3D modeling to model segmental tunnels under seismic loading and predicted their dynamic behavior in clayey soil [9]. The simulations revealed that adding multidirectional seismic loading to the tunnel increased longitudinal forces, a feature not included in bounded models. The consequences of their dynamic interaction with seismic excitation are studied using a two-dimensional plane model. Comparative analysis determines the law influencing the relationship between subterranean structures and soil. The findings indicate a relationship between the structure depth and the impact of the subterranean structure on the soil response. The surface response is significant within the range of the station structure's influence on the surface, around five times the station's breadth [10]. *Dong et al*. examined the longitudinal seismic capacity of shield tunnels. They determined that peak ground velocity (PGV) was appropriate for measuring longitudinal earthquake performance and that stronger seismic resistance was observed in the underlying EV phase. Using an earthquake (El Centro EW) as a seismic wave, researchers could simulate tunnel-lining displacement at the same site and observe the impact of the tunnel body on the acceleration response and soil liquefaction [11]. The study revealed that vertical stress increased at each monitoring point due to increased distance from the bottom of the shield tunnel under seismic loads, resulting in a decrease in vertical displacement and higher seismic wave peak acceleration. *Najm and Zakaria* looked at how tunneling processes and seismic impact affect the models of tunnels and the surrounding soil. Their results illustrate that stress decreases with distance[12]. During the dynamic phase, settlement increased in the tunnel zone. This comprehensive investigation combines advanced numerical modeling with theoretical analysis to provide deeper insights into the three-dimensional aspects of tunnel response that conventional two-dimensional analyses cannot capture. The results will have immediate practical applications for ongoing and future tunnel projects in seismically active regions. *Dong et al.* use the ANSYS software-implemented numerical simulation of tunnel soil to investigate the seismic response of the shield tunnel lining structure and suggest damping solutions [13]. The corners of the left and right walls experience the most stress, and the crown arch experiences the most deformation. This study's static and modal analyses used an EI Centro EW input forward 19 s seismic wave to assess the tunnel lining displacement, acceleration, and stress vibration parameters. The usefulness of this work extends beyond its theoretical use in tunnel engineering. It investigates isolation technologies and seismic reactions in a major utility tunnel segment with four compartments in a single layer; seismic simulations were conducted [14]. Through sophisticated three-dimensional numerical analysis using PLAXIS 3D, this study aims to (1) evaluate the seismic response of segmented tunnel linings under various earthquake conditions, with a particular focus on bending moment distribution and displacement patterns; (2) analyze the complex soil-structure interaction in layered soft clay conditions; and (3) assess the impact of different seismic characteristics on tunnel behavior. The findings will enhance design methodologies and construction practices for underground structures in seismically active regions with challenging soil conditions. This comprehensive investigation combines advanced numerical modelling with theoretical analysis to provide deeper insights into the three-dimensional aspects of tunnel response that conventional two-dimensional analyses cannot capture. The results of this study will have immediate practical applications for ongoing and future tunnel projects, particularly in regions characterized by soft soil conditions and significant seismic activity. This research addresses critical knowledge gaps in understanding segmented tunnel behavior during earthquakes, ultimately leading to more resilient underground infrastructure design.

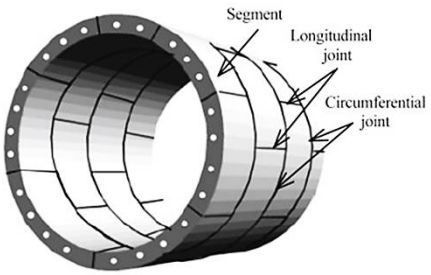

Figure1: Segmental tunnel lining
Source: journal of Rock Mechanics and Geotechnical Engineering

2. NUMERICAL MODEL

2.1. Soil Constitutive Model

The hardening Soil model is an advanced hyperbolic soil model formulated based on hardening plasticity [15]. It stimulates the soil behavior by defining three different moduli: the secant modulus for mobilization of 50% of maximum shear strength (E_{50}), the unloading-reloading modulus (E_{ur}), and the oedometer modulus (E_{oed}). The model considers soil dilation. The Hardening Soil model provides a more precise characterization of soil stiffness through three distinct input stiffness parameters: the triaxial loading stiffness (E_{50}), triaxial unloading stiffness (E_{ur}), and oedometer loading stiffness (E_{oed}). The default settings recommend that $E_{ur} \approx 3E_{50}$ and $E_{oed} \approx E_{50}$ are the average values for various soil types. However, different ratios for E_{oed} / E_{50} may be specified based on the characteristics of exceptionally soft or stiff soils. The Hardening Soil Model (HSM) is formulated based on the theory of plasticity, in contrast to the elasticity-based Duncan-Chang model [16]. The parameters of the Duncan-Chang model [17] can be readily obtained from a standard triaxial test. The HSM encompasses two distinct types of hardening: volumetric compression hardening, which models plastic strains arising from isotropic loading and primary compression in oedometer tests, and shear hardening, used to simulate strains resulting from primary deviatoric loading. Equation (1) presents the soil stiffness in the primary loading condition.

$$E_{50} = E_{50}^{ref}\left(\frac{\sigma_3^{'} + \cot\varphi}{p^{ref} + c\cot\varphi}\right)^{m} \quad (1)$$

Where:

$\boldsymbol{E_{50}}$**:** The stiffness modulus for mobilization of 50% of the maximum deviator stress (qf).

$\boldsymbol{E_{50}^{ref}}$**:** The reference stiffness modulus corresponding to a reference confining stress pref of 100 kPa.

$\boldsymbol{c}$ **&** $\boldsymbol{\phi}$: The shear strength parameters of the Mohr-Coulomb failure criterion.

$\boldsymbol{\sigma_3'}$: The effective confining pressure

$\boldsymbol{m}$: Power exponent.

E_{50} is used in the HSM instead of the initial tangent modulus (E_i) in the Duncan-Chang model since it is not easy to determine experimentally. A power law also describes the effect of unloading and reloading on the soil stiffness, as shown in equation (2).

$$E_{ur} = E_{ur}^{ref}\left(\frac{\sigma_3^{'} + c\cot\varphi}{p^{ref} + c\cot\varphi}\right)^{m} \quad (2)$$

Where:

$\boldsymbol{E_{ur}}$**:** The unloading-reloading stiffness modulus

$\boldsymbol{E_{ur}^{ref}}$**:** The reference unloading-reloading stiffness modulus corresponds to a reference confining stress p^{ref} of 100kPa. The ratio of the unloading-reloading and the primary loading moduli (E_{ur}/E_{50}) typically ranges from 3 to 10. It is similar to the compression and swelling indices (Cc/Cs) ratio measured in an oedometer test [18]. Cohesionless soils are usually characterized by (E_{ur}/E_{50}) of 2-3 [19], and cohesive soils are distinguished by larger ratios that may approach the upper limit of the spectrum, as previously noted. Another fundamental characteristic of the HSM is the consideration of the plastic straining due to primary compression, which can be defined as follows:

$$E_{oed} = E_{oed}^{ref}\left(\frac{\sigma_1' + c\cot\phi}{p^{ref} + c\cot\phi}\right)^{m} \quad (3)$$

Where:

$\boldsymbol{E_{oed}}$**:** The tangent stiffness modulus for primary loading.

$\boldsymbol{E_{oed}^{ref}}$**:** The reference tangent stiffness modulus corresponding to a reference vertical stress p^{ref} of 100 kPa

$\boldsymbol{\sigma_1'}$**:** The adequate vertical pressure

Schanz et al. (1999) mentioned that the HSM does not involve a fixed relation between E_{50} and E_{oed}, and these values should be determined independently[15]. The magnitude of the soil deformations is controlled in the HSM by three stiffness parameters that simulate loading (E_{50}), unloading-reloading (E_{ur}), and the oedometer loading conditions (E_{oed}^{ref}). In addition, the HSM accounts for the soil dilation by defining the initial void ratio (e_o) and the maximum void ratio (e_{max}) of the soil material. Compared to an elastic, perfectly plastic model, the yield surface of a hardening plasticity model is not fixed in principal stress space; it expands due to plastic straining. Two main types of hardening can be distinguished: shear hardening, used to simulate irreversible strains from primary deviatoric loading, and compression hardening, used for irreversible plastic strains from primary compression in oedometer loading and isotropic loading. The Hardening Soil model, developed by Shanz (1998), is an advanced tool for simulating the behavior of

various soil types, including both soft and stiff soils [20]. Under primary deviatoric loading, the soil experiences decreasing stiffness while irreversible plastic strains develop. In a drained triaxial test, the relationship between Axial strain and deviatoric stress closely approximate a hyperbola, as mentioned in (Kondner, 1963) and later incorporated into the well-known hyperbolic model [17, 21]. However, the Hardening Soil model surpasses the hyperbolic model in several ways: it utilizes the theory of plasticity over elasticity, includes soil dilatancy, and introduces a yield cap. A key aspect of this model is the stress-dependent soil stiffness. In cases involving soft soils, it is realistic to set m = 1, which also establishes a simple relationship between the modified compression index λ* and the oedometer loading modulus. Where p_{ref} is a reference pressure. Here, we consider a tangent oedometer modulus at a particular reference pressure, p_{ref}. Hence, the primary loading stiffness relates to the modified compression index λ^* or the standard Cam-Clay compression index λ as shown in equation (4).

$$E_{oed}^{ref} = \frac{p^{ref}}{\lambda^*} \qquad \lambda^* = \frac{\lambda}{(1+e_0)} \qquad (4)$$

2.2. Finite Element Model & Material Properties

In the case study of a shallow circular tunnel, the segments are lined with seven precast reinforced concrete segments of 2 m length and a key. The lining has an 8.35 m inside diameter and 400 mm thickness of lining segments, producing an external diameter of 9.15 m, according to tunnel boring machine (TBM) cutter head dimensions. The tunnel is under 10 m of soil cover. The damping ratio equals 5% according to the ASCE6-16 code for concrete material [22]. The hardening soil model is adapted for soil layers, while the lining is modeled as a linear visco-elastic material. The soil domain boundaries were placed at a minimum of 5 times the tunnel diameter away from the tunnel axis in both the horizontal (x and y) directions [23], so the model dimension is (100x50x60 m) as shown in Figure 2. The soil model parameter of the As shown in Table 1, the HS-Model used in this study was based on the values of the Geotechnical Characterization of Port-Said soft Clay [24]. The undrained condition was adapted for this model. Interface elements roughness coefficients (R_{inter}) were assigned as 1.0 for very smooth and soft clay layers (Clay1 and Clay2), 0.85 for firm clay layers (Clay3 and Clay4), and 0.67 for the fill and sand layers. The software assigns a Poisson's ratio of 0.30 in the undrained conditions. According to the borehole, the groundwater table is at zero level, under the ground surface by 2.5 m. Tunnel lining is represented using linear elastic elements with the assumed parameters, as shown in Table 2. The TBM shield is described as plate elements with the accepted parameters shown in Table 3 and a uniform contraction equivalent to 0.5% volume loss [25, 26].

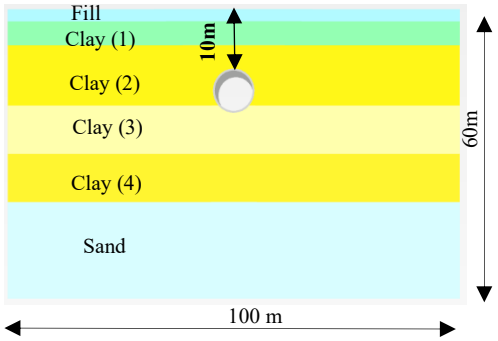

Figure 2: Soil layers & Model parameters for finite element model

Table 1. Soil parameters

layer	Level	γ_{sat} (KN/m³)	K_0	C' (kpa)	φ′ (degree)	E_{50}^{ref} (Mpa)	E_{oed}^{ref} (Mpa)	m
fill	+2.50	17	0.52	0	29	20	20	0.5
Clay1	-5.50	16	0.59	0	22	4.66	2.1	0.81
Clay2	-17.5		0.64					
Clay3	-27.5		0.68					
Clay4	-37.5		0.72					
sand	-57.5	18	0.43	0	35	30	30	0.5

Where:

***K₀*:** value for standard consolidation.

***C′*:** Effective cohesion.

φ′: Effective angle of internal friction.

$\boldsymbol{E_{50}^{ref}}$**:** Secant stiffness in standard drained triaxial test.

$\boldsymbol{E_{oed}^{ref}}$**:** Tangent stiffness for primary oedometer loading.

m: Power for the stiffness's dependence on stress level.

Table 2. Concrete material properties representing the tunnel lining.

Parameter	Lining	unit
Unit weight (γ_{unsat})	27	kN/m³
Young's modulus (E')	$1.4*10^7$	kpa
Poisson's ratio (v')	0.15	-
Interface strength(R_{INTER})	Rigid	-

Table 3. Material properties of the TBM shield.

Parameter	TBM	Unit
Thickness (d)	0.14	m
Material weight (γ)	120	KN/m³
Young's modulus (E1)	$2*10^8$	kpa
Poisson's ratio (v12)	0.3	-
Shear modulus (G12)	10^8	kpa

2.3. Ground Motion Characteristics

The earthquake data was obtained from the different stations during the seismic events in many

places in the United States of America. The El Centro Earthquake of 18 May 1940 & the Petrolia Earthquake of 26 April 1992, and the Geysers, California Earthquake of 15 July 2010 are utilized for analysis, as depicted in Figure 3 and Figure 4. The general characteristics of the selected seismic motions are summarized in Table 4. Pseudo-Spectral Acceleration (PSA) is a reliable estimator of seismic loading for a broad range of structures. It is defined as the absolute maximum response of a single-degree-of-freedom oscillator (SDOF) to an input ground motion. The dynamic analyses are conducted under undrained conditions, employing a time step corresponding to the earthquake input signals. Viscous boundaries are chosen on both sides of the x-direction for the earthquake phase, none are selected for the other sides, and a compliant base option is chosen for the model bedrock in which the seismic force is applied. The effective duration of the input motion, set at 20 seconds, is adapted for analysis in each phase. The seismic response analysis incorporated three distinct earthquake events with varying characteristics to evaluate tunnel behavior under different loading conditions. The El Centro earthquake (Mw 6.9) exhibited moderate intensity with a peak ground acceleration of 0.25g and a maximum velocity of 29.078 cm/s at an epicentral distance of 16.9 km. Its response spectrum showed consistent energy distribution with gradual decay over the period range, while its acceleration time history demonstrated sustained ground motion over approximately 30 seconds. The Petrolia earthquake (Mw 7.2) represented the most severe seismic event, with significantly higher peak ground acceleration (1.427g) and maximum velocity (269.393 cm/s) at an epicentral distance of 42.0 km. Its response spectrum revealed substantial energy content across multiple periods, with a peak spectral acceleration of approximately 4.0g. In contrast, the Geysers earthquake (Mw 4.0) displayed the lowest intensity, with peak ground acceleration of 0.086g and maximum velocity of 1.647 cm/s at an epicentral distance of 10.5 km, characterized by a concentrated burst of high-frequency content and rapid amplitude decay in both its response spectrum and acceleration time history. These distinct seismic characteristics directly influenced the observed variations in tunnel response, particularly evident in the case of the Petrolia earthquake, where the combination of high magnitude and sustained strong motion resulted in the most significant structural impacts.

Table 4. Characteristics of the studied Earthquakes.

NO.	Earthquake	Magnitude (Mw)	Epicentral distance (km)	a_{max} (g)	v_{max} (cm/s)
1	El Centro	6.9	16.9	0.25	29.078
2	Petrolia	7.2	42.0	1.427	269.393
3	The Geysers	4.0	10.5	0.086	1.647

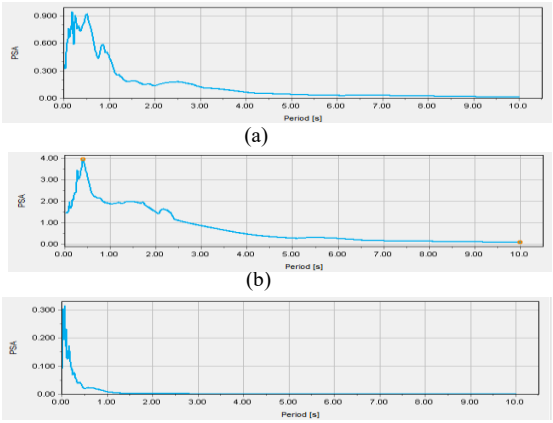

(a)

(b)

(c)

Figure 3: Input motions response spectra; a) El Centro Earthquake, b) Petrolia Earthquake and c) The Geysers Earthquake

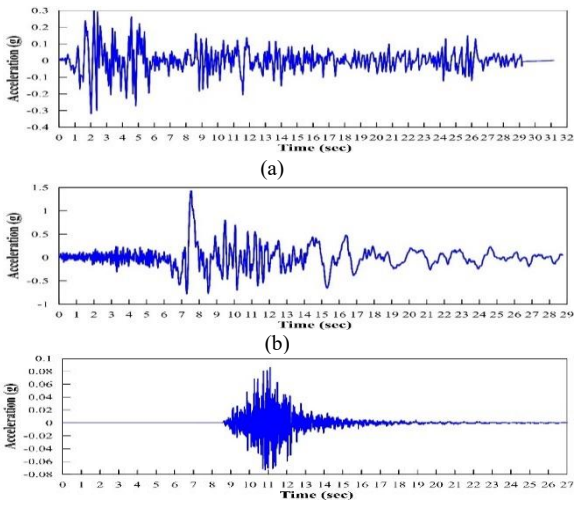

(a)

(b)

(c)

Figure 4: Input the motion acceleration time history; a) El Centro Earthquake, b) Petrolia Earthquake and c) The Geysers Earthquake

2.4. Mesh Generation

The mesh for the tunnel is shown as a finer mesh in Figure (5) with a total number of elements of 65027 and 103907 nodes. The grid used for the three-dimensional finite element is the tetrahedral elements 10-node, which is also used for tunnel-lining modeling. The interface elements com/bine pairs of nodes matching the 6-point trigonometric side of the plate or soil element [23]. Mechanical boundary conditions at X_{min}, X_{max}, Y_{min}, and Y_{max} are usually fixed, Z_{min} is fully fixed, and Zmax is free. Flow boundary condition X_{min}, X_{max}, Y_{min}, Y_{max}, Z_{max} closed and Z_{min} open.

Table 5. Studied cases for model simulation.

Phase. NO	PHASE NAME	PHASE CONDITION
1	EXCAVATION	undrained condition
2	LINING (STATIC PHASE)	
3	APPLY EARTHQUAKES IN THE X-DIRECTION FORCE	

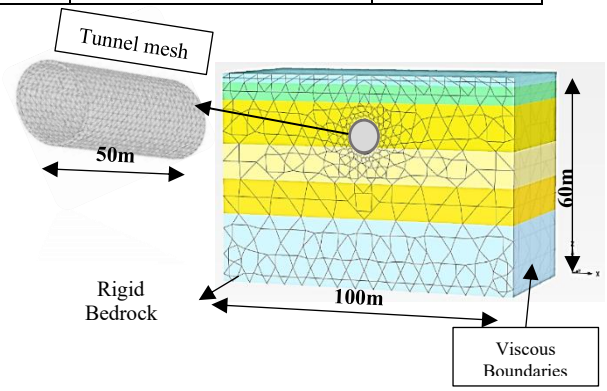

Figure 5: Model mesh of tunnel-soil

Model Sections and Study Cases

The modeling process contains three phases: the first one is excavation, the second is the lining process, and the third one is earthquake modeling. The earthquake motion phase is applied in the x-direction (in the direction perpendicular to the tunnel axis), as shown in Table (5). The hardening soil model (HSM) is employed to demonstrate the behavior of soil-structure interaction in the soil surrounding the tunnel and the soil failure criteria from the results. To distinguish between the stress deformation of the tunnel segment lining caused by the displacement of seismic waves, the action of gravity, the surrounding soil, and the deformation of the tunnel lining. Understanding the changes in the tunnel lining due to gravity is essential before undertaking the dynamic time history analysis. The datum of the middle of the tunnel section (1-1) & Section (2-2) is located at 5m from the (1-1) section, and section (3-3) is located at 10m from section (1-1), as shown in Figure (6). Section (B-B) is above tunnel lining & section (A-A) is above section (B-B) by 9 m.

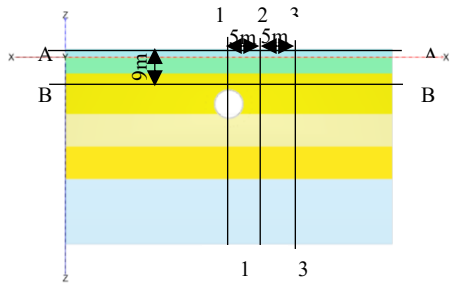

Figure 6: Displaying location of sections taken from tunnel model

3. RESULTS AND DISCUSSIONS

3.1. Vertical Displacement Distribution Along The Depth

Figure (7) shows the analysis of vertical displacement under static and seismic conditions, revealing distinct patterns at cross-section (1-1). The Petrolia earthquake has the most significant impact, creating the largest settlement zone and extensive deformation patterns in the surrounding soil. The El Centro earthquake generates moderate settlement at the tunnel lining, with displacement magnitudes less severe than Petrolia but more pronounced than Geysers. The Geysers earthquake exhibits the least impact, with maximum and minimum displacement values at 0 mm, indicating a more uniform soil response pattern. At cross-section (2-2), the analysis shows persistent vertical displacement activity adjacent to the tunnel lining, development of soil heaving phenomena beyond the tunnel structure, complex interaction patterns between the tunnel and surrounding soil matrix, and distinct zones of influence extending from the tunnel periphery. Section (1-1) shows more sensitivity to seismic loading conditions than Section (2-2). In sec (2-2), we can see that the vertical displacement is still active besides the tunnel lining. This comprehensive analysis demonstrates the varying degrees of seismic impact on tunnel stability and ground response, with the Petrolia earthquake generating the most significant deformation patterns. The maximum displacement caused by the Petrolia earthquake was equal to 299 mm, as shown in Figure (8).

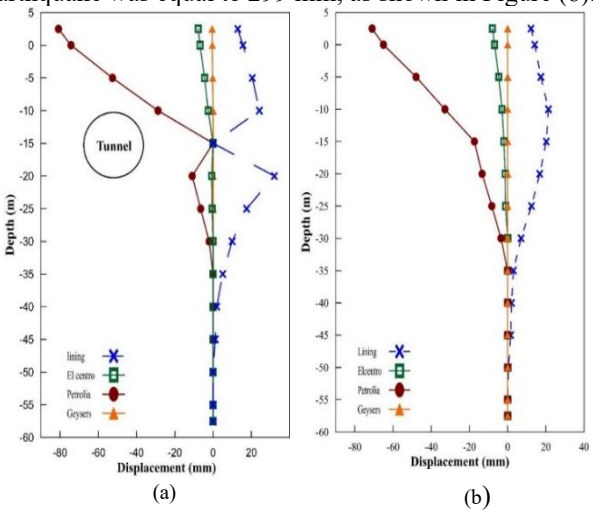

Figure 7: Distribution of the vertical displacement; a) cross section (1-1) and b) cross section (2-2)

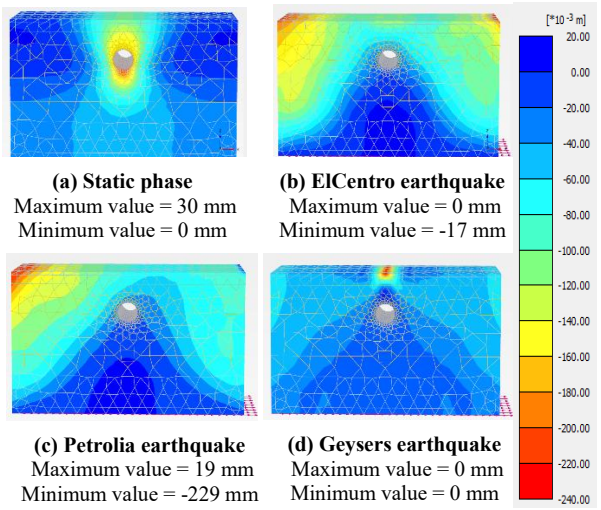

Figure 8: Vertical displacement values for all phases

3.2. Vertical Displacement According to Dynamic Time

Figure (9) demonstrates the maximum settlement observed during the dynamic analysis of temporal patterns in vertical displacement under seismic loading conditions. The El Centro earthquake exhibited a maximum displacement of approximately 0.05 meters, with a stable response after initial oscillations. In contrast, the Petrolia earthquake experienced the most significant displacement, around 0.08 meters, causing severe progressive deformation and significant impacts on tunnel structures due to continuous increases in displacement over time. Meanwhile, the Geysers earthquake showed minimal displacement of about 0.0001 meters, characterized by high-frequency oscillations and better structural resilience owing to its more elastic response behavior. These observations underscore the critical importance of designing infrastructure capable of adapting to various seismic intensities and behaviors. A notable contrast in behavior is evident in examining the displacement and acceleration responses of these three sites—El Centro, Petrolia, and Geysers. The El Centro site exhibits a maximum crown displacement of approximately 0.045 meters, characterized by a steady increase over the initial 5 seconds, followed by gradual stabilization after 10 seconds. Other sections (left, right, and bottom) show similar, albeit reduced, displacement patterns, indicating a more uniform settlement trend. In contrast, the Petrolia site demonstrates larger displacement magnitudes, reaching up to 0.065 meters. The crown section experiences the most significant movement, with a more irregular displacement pattern persisting over a 20-second and more substantial variation between different tunnel sections. The Geysers site presents minimal displacement at around 0.00012 meters, with high-frequency oscillations and a more uniform response across all sections, rapidly returning to a stable condition. Regarding acceleration, El Centro has a peak acceleration of ±0.3g, with sustained ground motion over approximately 30 seconds, displaying a regular wave pattern with moderate amplitude variations. Petrolia records the highest peak acceleration of ±1.5g, characterized by a strong initial pulse at around 8 seconds, longer significant motion duration, and a more irregular acceleration pattern. Conversely, Geysers show a peak acceleration of ±0.08g, with a concentrated burst of energy between 8-12 seconds, a short duration of strong motion, and high-frequency content. These varied responses highlight how different seismic events can uniquely affect structural integrity, emphasizing the need for robust engineering solutions that ensure safety and functionality in the face of unpredictable natural forces. The Petrolia earthquake generated the most severe structural response due to its higher acceleration amplitude and longer intense motion duration. In contrast, despite its high-frequency content, the Geysers earthquake had minimal impact on the tunnel structure.

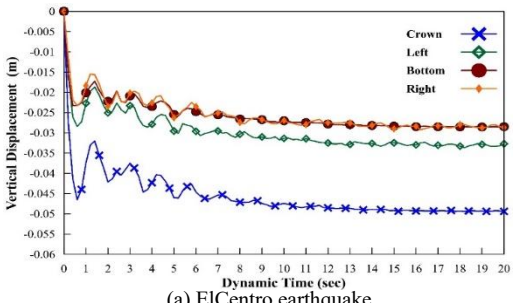

(a) ElCentro earthquake

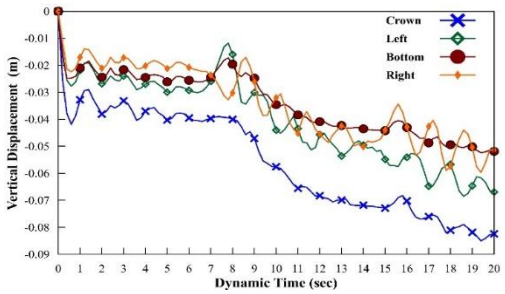

(b) Petrolia earthquake

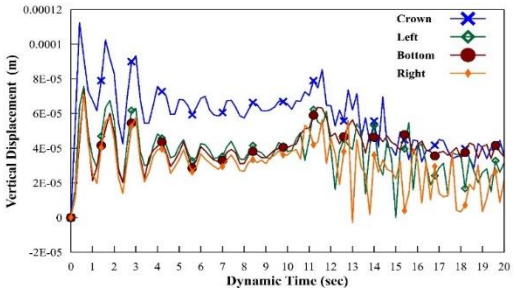

(c) Geysers earthquake

Figure 9: Tunnel cross sections vertical displacement according to dynamic time

3.3. Vertical Displacement Distribution Along Horizontal Sections

Figure (10) Comparative vertical displacement distribution along horizontal cross-sections A-A and B-B under different loading conditions. Under various conditions, studying vertical displacement patterns in two soil sections (A-A and B-B) will give us information about structural integrity and soil stability. Under static conditions, minimal displacement (±10 mm) is observed with slight upward movement at the tunnel's center. The El Centro earthquake induces moderate downward displacement (-40 mm) at 40-60 m tunnel location. The Petrolia earthquake caused severe progressive settlement, with a maximum of -200 mm at the beginning and -80mm at the end of the model. The Geysers earthquake has minimal impact, similar to static condition. Section B-B has a more uniform displacement pattern under all conditions. The Petrolia earthquake caused maximum settlement (-160 mm) to be distributed all over, and the El Centro earthquake showed local settlement (-50 mm) at a 50m tunnel location. Both the Static lining and Geysers condition are stable with minimal displacement. Petrolia earthquake causes more vertical displacement in both sections, and the displacement pattern is different; it's 3D response. Maximum settlement is at various locations within each section, El Centro is concentrated at the tunnel's center, and Petrolia is at the entire length. The soil above the tunnel is displaced more than near the ground. Overall, the earthquake characteristics will affect the magnitude and pattern of vertical displacement, the tunnel's structural integrity, and the surrounding soil's Stability.

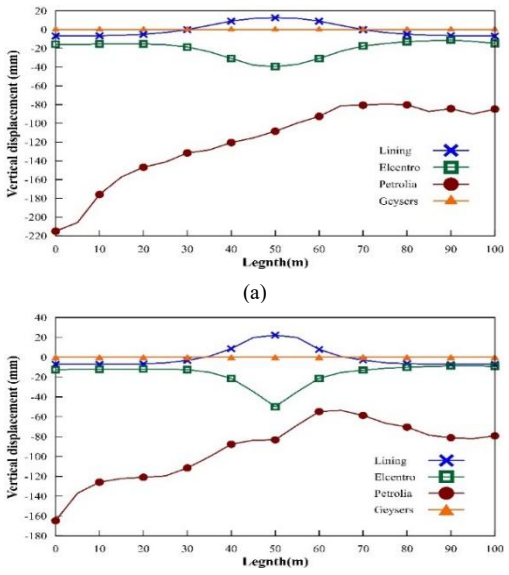

Figure 10: Distribution of the Vertical displacement ; a) cross section (A-A) and b) cross section (B-B)

3.4. Horizontal Displacement Distribution Along Horizontal Sections

Figure (11) Shows that the horizontal displacement distribution analysis reveals distinct behavioral patterns between sections (A-A) and (B-B) under various seismic loading conditions. The Petrolia earthquake induced the most substantial displacements, exhibiting a Nonlinear increase with length, reaching maximum values of approximately 200 mm at 90 m in sections (A-A) and 220 mm in sections (B-B). This marked difference from other loading conditions (Static Lining, El Centro, and Geysers), which maintained minimal displacements of 10-20 mm, can be attributed to several key mechanisms: (1) the differential soil confinement effects at varying depths, where deeper soil layers experience higher confining pressures leading to sustained displacement; (2) wave propagation characteristics, with seismic waves maintaining energy longer in confined conditions; and (3) the tunnel structure's influence as a barrier, creating distinct displacement behaviors in the surrounding soil. Section A-A demonstrates a more complex displacement pattern with three distinct phases: rapid initial increase (0-20 m), plateau (20-60 m), and a sharp increase (60-90 m), while section B-B shows a more uniform, gradual progression of displacement with length. This behavior suggests that the tunnel's response to seismic loading varies significantly along its alignment, influenced by the combined effects of soil-structure interaction and wave propagation mechanisms. These findings show the importance of considering spatial variations and depth-dependent responses in the seismic design of underground structures.

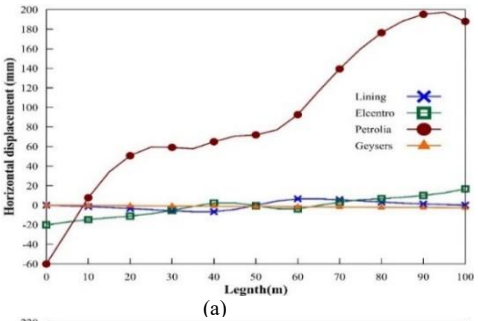

(a)

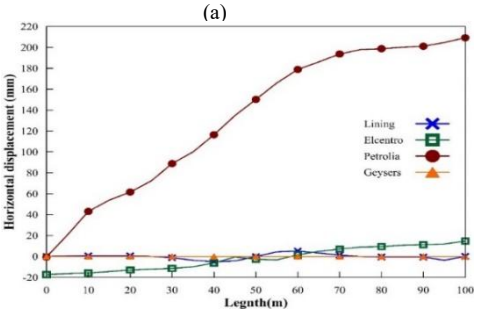

(b)

Figure 11: Distribution of the Horizontal displacement; a) cross section (A-A) and b) cross section (B-B)

3.5. Horizontal Displacement According to Dynamic Time

Figure (12) presents the horizontal displacement (Ux) observed at section (1-1), which is located 25 meters from the tunnel's start point. During the Petrolia earthquake, specifically at the eighth second, the tunnel lining experienced a substantial deformation, recorded at -60 mm in the x-direction. This deformation continued to evolve, reaching its maximum extent of 180 mm by the twentieth second. The impact of the El Centro earthquake was particularly significant on the right and left sides of the tunnel lining, with these areas experiencing 67% more deformation than the crown and bottom of the tunnel section. On the other hand, the Geysers earthquake did not have a noticeable effect on the crown and bottom of the tunnel. However, it did impact the left and right sides of the tunnel lining. The differential effects of the various earthquakes on the tunnel lining are attributed to the distinct magnitudes of the earthquakes and their respective natural frequencies. Each earthquake's unique characteristics determined the deformation patterns observed in the tunnel lining, highlighting the importance
seismic activity should be considered in the design and analysis of tunnel structures [27].

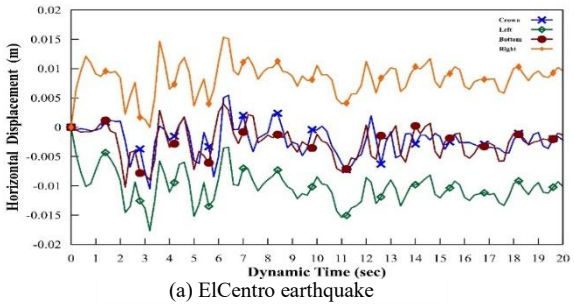

(a) ElCentro earthquake

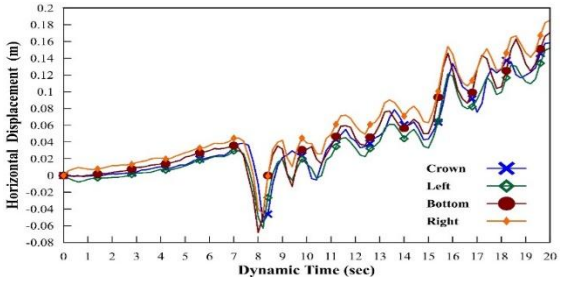

(b) Petrolia earthquake

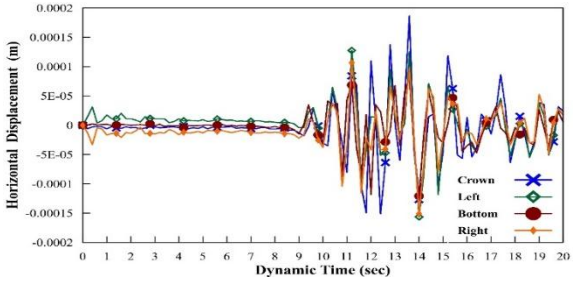

(c) Geysers earthquake

Figure 12: Tunnel cross sections horizontal displacement (Ux) according to dynamic time

3.6. Horizontal Displacement Distribution Along the Depth for Petrolia Earthquake

The location of the tunnel lining exhibits a significant displacement of approximately 180 mm due to the presence of soft clay soil and the groundwater table above the tunnel lining. In Figure (13), we can see that the displacement above the tunnel of the soil records a maximum displacement equal to 150 mm; the horizontal displacement increases in sec (2-2) & (3-3). The horizontal displacement decreases after tunnel lining and is stable at a depth of 40m. Critical depth has been observed after 20m from the tunnel lining; the tunnel lining may affected by the Rayleigh wave [28]. Figure (14) illustrates the horizontal displacement distribution for the three sections (1-1), (2-2), and (3-3). After twenty seconds from the earthquake, it is observed that the soil in sections (3-3) moves in the x-direction more than the other sections. This phenomenon may be attributed to the tunnel, causing the soil to become stiffer. As we move further from the tunnel, the soft clay is more affected by the earthquake, which denotes that the tunnel embedded at 10 m overburden depth experienced considerably more seismic-induced deformation and structural forces than the tunnel buried at 20 m depth [29].

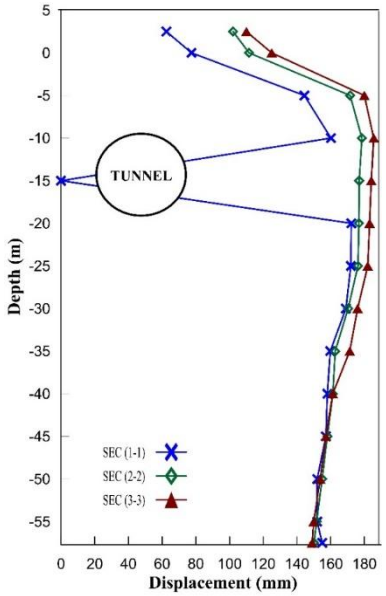

Figure 13: Horizontal displacement distribution for sections according to Petrolia earthquake

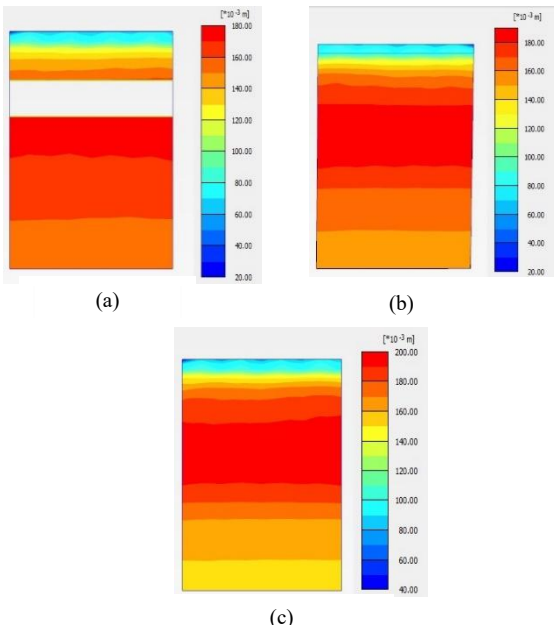

Figure 14: cross sections for horizontal displacement (Ux) according to Petrolia earthquake; a) cross section (1-1), b) cross section (2-2) and c) cross section (3-3)

3.7. Pore Water Pressure Distribution

Significant variations in maximum pore pressure and pressure distributions were evident when comparing the initial phase with the conditions observed during three earthquake events. The initial phase exhibited a maximum pore pressure of 2.22 kN/m². During the El Centro earthquake, there was a slight increase in maximum pore pressure to 2.67 kN/m², with a relatively uniform pressure distribution and a more stable pressure gradient with depth, indicating a moderate impact on soil-water interaction. In contrast, the Petrolia earthquake recorded the highest maximum pore pressure at 14.12 kN/m², resulting in the most significant effect on pressure distribution, greater pressure fluctuations around the tunnel, and a substantial deviation from initial conditions, highlighting considerable stress on tunnel structures. The Geysers earthquake presented the lowest maximum pressure of 1.75 kN/m² and the most significant negative pressure of -571.12 kN/m², indicating the most extreme pressure variation and considerable pressure reduction in certain zones. These variances can be related to variations in wave characteristics, such as frequency content affecting soil-water interaction, wave propagation patterns influencing pressure distribution, and the duration of seismic loading impacting pressure buildup.

Additionally, the soil response plays a crucial role, where cyclic loading causes changes in soil structure, void ratio variations affect pressure distribution, and soil permeability alters during seismic events. In sec (2-2), we can see the pore water pressure along the whole model depth besides the tunnel lining. The tunnel influence is also significant; the presence of the tunnel creates pressure concentration zones, structural rigidity affects pressure redistribution and interface conditions influence pressure transmission. These observations align with recent geotechnical research findings regarding seismic effects on pore water pressure in tunnel environments, emphasizing the need for robust engineering designs that consider these factors to ensure the integrity and resilience of underground structures during seismic events, as shown in Figure (15). Values of pore water pressure for all phases show the maximum and minimum tunnel position, as shown in Figure (16).

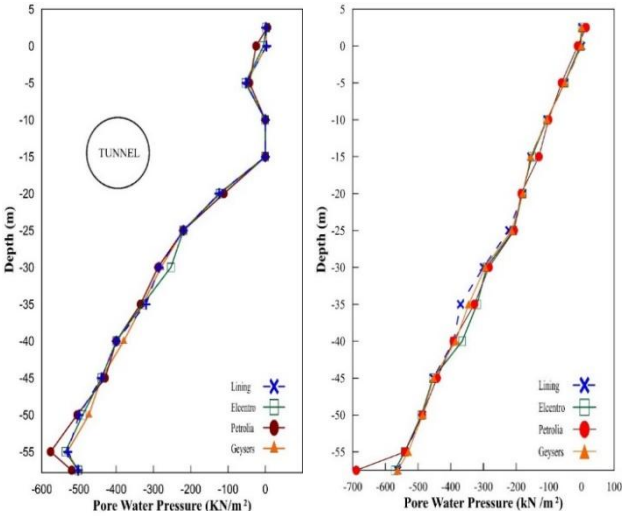

Figure 15: Distribution of the pore water pressure; a) cross section (1-1) and b) cross section (2-2)

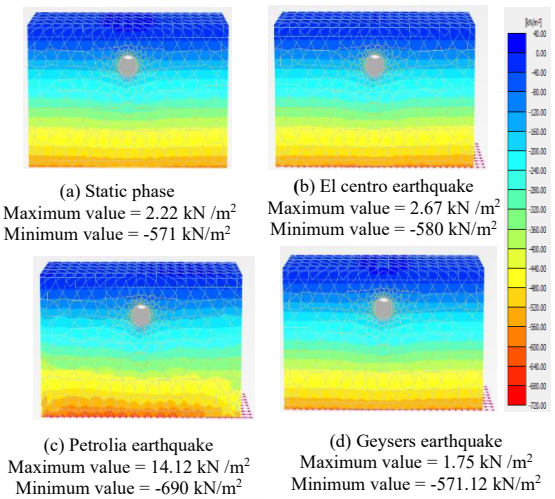

Figure 16: pore water pressure minimum & maximum values for all phases

3.8. Bending Moment Distribution Along The Tunnel Lining

Figure (17) shows the bending moment distribution along the tunnel's length on the tunnel's rings after 20 seconds from each earthquake. The analysis of the static lining phase indicated a relatively uniform distribution of bending moments, with values at the crown, invert, and springline being -63 kN.m, -51 kN.m, and 65 kN.m, respectively. The analysis of the El Centro earthquake response showed a very high rise in bending moments, reaching up to 85%, to result in values of -117 kN.m at the tunnel crown, -90 kN.m at the invert, and ranging between 110 and 114 kN.m at the sides of the tunnel. The Petrolia earthquake had the most severe impact, demonstrating a significant increase from the static condition, with moments of -300 kN.m at the crown, -290 kN.m at the invert, and 307 kN.m at the tunnel sides. In contrast, the Geysers response was similar to the static phase, with minimal variation and values of -63.67 kN.m at the crown and -51 kN.m at the invert. The longitudinal distribution analysis revealed that the maximum moment occurred at approximately 12 meters in length, with significant variations between 20 to 40 meters and divergent behavior at the terminal section. Structural design considerations should account for Petrolia-type events, with joint spacing, flexibility, and reinforcement distribution reflecting moment variation patterns. These findings align with recent research on seismic wave propagation and soil-structure interaction in underground structures, as shown in Figure (17). The difference in bending moment happens due to the tunnel lining position according to earthquakes resonance with tunnel neutral frequency; the effect of earthquakes on tunnel lining had taken it x-direction (the weak side of the tunnel). Figure (18) illustrates how the bending moment on rings is distrustful in every phase, and the section taken according to the studding model is a 25 m long tunnel length from the tunnel's beginning.

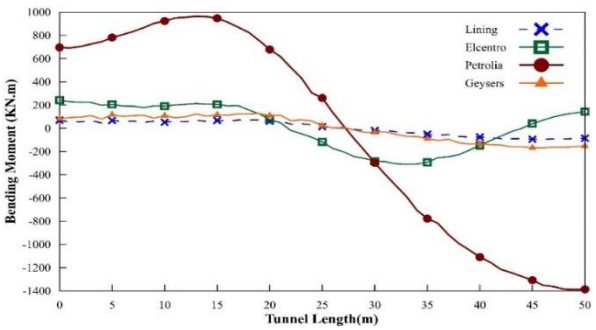

Figure 17: Distribution of bending moment along the tunnel lining

Table 6. Magnitude of maximum displacement in vertical& horizontal direction.

Load cases for tunnel	Maximum total displacement in UZ (mm)	Maximum total displacement in UX (mm)	Maximum total displacement in UY (mm)
Static phase	30	11	0
El Centro earthquake	50	25	0
Petrolia earthquake	231	254	0
Geysers earthquake	38	8	0

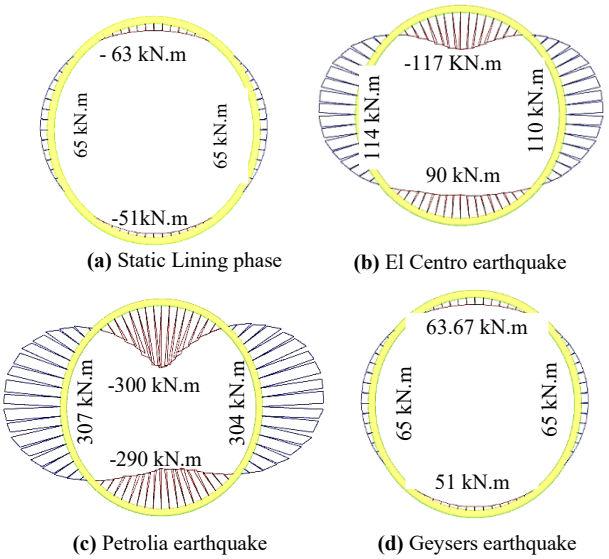

(a) Static Lining phase **(b)** El Centro earthquake

(c) Petrolia earthquake **(d)** Geysers earthquake

Figure 18: Bending moment distributions on tunnel rings at 25m

3.9. Surface Settlement And Maximum Displacement Under Static Phase And Earthquake Load Cases.

The analysis of tunnel response under various seismic conditions reveals significant variations in displacement patterns, strongly influenced by soil stratigraphy and earthquake characteristics. The finite element model, incorporating multiple clay layers with varying properties (Clay1-Clay4) and a total depth of 60m, demonstrates maximum displacements ranging from minimal to substantial depending on the seismic input. Ground movements with tunnel lining and the surrounding soil. It compared tunnel lining (static condition) and the effect on earthquakes for every caseload of dynamic loading. From the model results analysis, the settlement in the soil at the lining phase (initial phase) is the maximum displacement of 30 mm in the vertical direction. Settlement of the El Centro Earthquake is recorded at 50 mm; this may cause cracks at the bottom and upper of the tunnel. The Petrolia Earthquake recorded 231 mm at the vertical plane, while the horizontal plane recorded 254 mm. Geyser earthquake does not record any change in tunnel lining; the maximum displacement recorded by the Petrolia Earthquake equals 231 mm as settlement and may cause cracks for the sides of the tunnel and bottom and upper. Therefore, the Petrolia earthquake affected the vertical plane of the tunnel more than the earthquake in El Centro. Petrolia Earthquakes affect the horizontal plane more than the vertical plane, as shown in Table (6). These findings illustrate the critical importance of considering both the soil stratigraphy and seismic motion characteristics in tunnel design, particularly in layered soft soil conditions where displacement magnitudes can vary significantly based on the input motion characteristics.

4. CONCLUSIONS

This paper concentrates entirely on the effect of the earthquake on segmental tunneling on soft clays. It could be seen from the results that:

1. The impact of the Petrolia earthquake on the tunnel lining is more significant than any other earthquake due to the high settlement caused by the considerable intensity content in the seismic wave. In addition, the overlying soil by 231 mm greater than the settlement caused by other earthquakes, such as the El Centro earthquake (50 mm).
2. The soil displacement at cross-section (A-A) and cross-section (B-B) is nearly equal and uniformly distributed. Indicates that the effect of tunnel depth on seismic response is not evident, except in the case of shallow tunnels, which are affected by surface Rayleigh waves.
3. High-frequency earthquakes can induce significant changes in pore water pressure throughout the soil profile, resulting in a substantial settlement in soft soils. In the case of the Petrolia earthquake, the pore water pressure at the top of the soil model value equals 14.12 kN/m2, more than that of other seismic waves.
4. The crown of the tunnel experiences the highest degree of displacement, with a 33% greater impact than the two sides (left & right) and bottom Consequently, increasing the reinforcement in this section of the tunnel lining according to the tunnel bending moment caused by the earthquake is advisable to enhance its structural integrity.
5. The Geysers earthquake does not influence the crown and bottom but affects the tunnel's left and right sides. These observations suggest that earthquakes influence the segmental tunnel lining in various ways, depending on their magnitude and natural frequency.
6. When the tunnel's depth exceeds the critical depth, the horizontal displacement diminishes as the burial depth of the structure increases. As

for the Rayleigh wave, the maximum acceleration occurs at critical depth but not at the ground surface, as people generally think.

It should be noted that the findings of this study are based on a fixed tunnel geometry (diameter and depth) and a limited number of earthquake records. Therefore, while the results provide valuable insight into the influence of seismic wave characteristics on tunnel performance in soft soil, caution should be exercised in generalizing the conclusions to all tunnel systems. Further studies varying tunnel size, depth, and soil profiles are recommended to support broader generalization.

5. STATEMENTS & DECLARATIONS

The authors declare that no funds, grants, or other support were received during the preparation of this manuscript.

6. REFERENCES

[1] Guan, Z., T. Deng, G. Wang, and Y. Jiang, Studies on the key parameters in segmental lining design. Journal of Rock Mechanics and Geotechnical Engineering, 2015. 7: p. 674-683.

[2] Brinkgreve, R., E. Engin, and W. Swolfs, PLAXIS 3D 2013 user manual. Plaxis bv, Delft, 2013.

[3] Buckle, I.G., R.L. Mayes, and M.R. Button, Seismic Design and Retrofit Manual for Highway Bridges. Federal Highway Administration, 1987. FHWA-IP-87-6.

[4] Chun-Shan, Y., H. Mo, C. Jun-Sheng, and W. Yi-Zhao, Influence of Seismic Loading on Segment Opening of a Shield Tunnel. TheScientificWorldJournal, 2014. 2014: p. 387210.

[5] Gharehdash, S. and M. Barzegar, Numerical modeling of the dynamic behaviour of tunnel lining in shield tunneling. KSCE Journal of Civil Engineering, 2015. 19.

[6] Zheng, J., C. Qi, Y. Xu, and K. Li, Nonlinear Dynamic Responses of Tunnels under Longitudinal Seismic Actions. 2014. 532-539.

[7] Mohammed, J., NUMERICAL MODELLING FOR CIRCLE TUNNEL UNDER STATIC AND DYNAMIC LOADS (CASE STUDY: COMPARISON IN DIFFERENT OF ELASTIC MODULUS AND TUNNEL DIAMETERS). 2017.

[8] Chen, G., et al., Nonlinear Response Characteristics of Undersea Shield Tunnel Subjected to Strong Earthquake Motions. Journal of Earthquake Engineering, 2018. 24:3, 351-380.

[9] Cabangon, L., G. Elia, and M. Rouainia 3D Numerical Analysis of Tunnel Behaviour in Clayey Soils under Seismic Loads. 16th European Conference on earthquake engineering, Thessaloniki, 2018.

[10] Sun, F., et al., Seismic Response Study of Tunnels Running underneath a Subway Station in Parallel. Shock and Vibration, 2020. 2020(1): p. 8822981.

[11] Dong, Z., et al., Examination of Longitudinal Seismic Vulnerability of Shield Tunnels Utilizing Incremental Dynamic Analysis. Frontiers in Earth Science, 2021. 9: p. 779879.

[12] Najm, N. and W. Zakaria, Predicting of Seismic Performance on Tunnel in Weak Soil. Diyala Journal of Engineering Sciences, 2023: p. 16-29.

[13] Dong, S., et al., Study on Seismic Response and Vibration Reduction of Shield Tunnel Lining in Coastal Areas. Sustainability, 2023. 15: p. 4185.

[14] Wang, Z., et al., Seismic isolation technology of shallow buried large section utility tunnel with soft soils in seismically vulnerable area. Frontiers in Earth Science, 2024. 12.

[15] Schanz, T., P. Vermeer, and P. Bonnier, Formulation and verification of the Hardening-Soil Model. 1999.

[16] Kok, S., et al., A Review of Basic Soil Constitutive Models for Geotechnical Application. Electronic Journal of Geotechnical Engineering, 2009. 14.

[17] Duncan, J. and C.-Y. Chang, Nonlinear Analysis of Stress and Strain in Soils. Proc. Paper: J Soil Mech and Found Division ASCE, 1970. 96: p. 1629-1653.

[18] Obrzud, R., On the use of the Hardening Soil Small Strain model in geotechnical practice. Elmepress International, 2010.

[19] Yong, C., Modelling ground response for deep excavation in soft ground. International Journal of Geomate, 2016. 11.

[20] Schanz, T., Zur Modellierung des mechanischen Verhaltens von Reibungsmaterialien. 1998.

[21] Kondner, R., Hyperbolic Stress-Strain Response: Cohesive Soils. Journal of the Soil Mechanics and Foundation Division ASCE, 1963. 89: p. 115-143.

[22] Cabangon, L., G. Elia, and M. Rouainia, 3D Numerical Analysis of Tunnel Behaviour in Clayey Soils under Seismic Loads. 2018.

[23] Brinkgreve, R.B.J. and M. Post, On the use of finite element models for geotechnical design. Bernessen mit numerischen methoden Workshop 2013. Veroffentlichungen des Institutes, 27.

[24] Hamed, O., M. Mansour, A. Abdel-Rahman, and F. El-Nahhas, Geotechnical Characterization of Port-Said Clay. 2017.

[25] Hamza, M. and H. Hamed, Three Dimensional Soil-Structure Analysis of Port-Said East Quay

Wall. Vol. 51: 371-380. 2000, WIT Transactions on The Built Environment.

[26] El-Nahhas, F., M. Y.M.El, and A. El-Shamy, 3D ANALYSIS OF GROUND SETTLEMENT INDUCED BY MECHANIZED TUNNELLING. Vol. Session 11. 2015, Ain Shams University: The Fourteenth International Conference on Structural and Geotechnical Engineering (ICSGE 14).

[27] Kouretzis, G., G. Bouckovalas, and D. Karamitros, Seismic verification of long cylindrical underground structures considering Rayleigh wave effects. Tunnelling and Underground Space Technology, 2011. **26**: p. 789-794.

[28] Xu, Y., C. Qi, and G. Chen, *The Effect of Structure Bury Depth on Dynamic Response of Underground Tunnel under Longitudinal Shearing Seismic Action.* Advanced Materials Research, 2014. **1020**: p. 415-422.

[29] Fazully, F., S.K.C. Osmi, M. Othman, and N. Hafizi, *Seismic Response of Tunnels Under Effect of Overburden Depth Using Simplified Pseudo-Static Analysis.* Jurnal Kejuruteraan, 2025.